ACS NANO

www.acsnano.org

ARTICLE

Composite Supraparticles with Tunable Light Emission

Federico Montanarella,[†,‡] Thomas Altantzis,[§] Daniele Zanaga,[§] Freddy T. Rabouw,[‡] Sara Bals,[§] Patrick Baesjou,[‡] Daniel Vanmaekelbergh,[*,†] and Alfons van Blaaderen[‡]

[†]Condensed Matter and Interfaces and [‡]Soft Condensed Matter, Debye Institute for Nanomaterials Science, Utrecht University, P.O. Box 80000, 3508 TA Utrecht, The Netherlands

[§]EMAT, University of Antwerp, Groenenborgerlaan 171, B-2020 Antwerp, Belgium

Supporting Information

ABSTRACT: **Robust luminophores emitting light with broadly tunable colors are desirable in many applications such as light-emitting diode (LED)-based lighting, displays, integrated optoelectronics and biology. Nanocrystalline quantum dots with multicolor emission, from core- and shell-localized excitons, as well as solid layers of mixed quantum dots that emit different colors have been proposed. Here, we report on colloidal supraparticles that are composed of three types of Cd(Se,ZnS) core/(Cd,Zn)S shell nanocrystals with emission in the red, green, and blue. The emission of the supraparticles can be varied from pure to composite colors over the entire visible region and fine-tuned into variable shades of white light by mixing the nanocrystals in controlled proportions. Our approach results in supraparticles with sizes spanning the colloidal domain and beyond that combine versatility and processability with a broad, stable, and tunable emission, promising applications in lighting devices and biological research.**

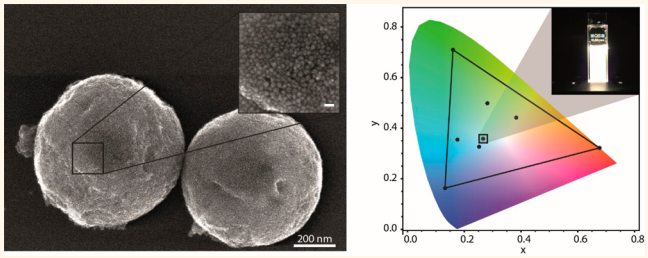

KEYWORDS: *quantum dot, nanocrystal, assembly, supraparticles, tunable emission, white light*

Even after more than two decades of extensive research, the optical properties of colloidal semiconductor nanocrystals, also known as quantum dots (QDs),[1] continue to intrigue researchers in nanophotonics, materials science and biology. Compared to solid-state QDs, colloidal QDs have a smaller and more easily tunable size.[2] This means that, due to strong exciton confinement, the light emission is tunable over a wide wavelength range in the visible or near-IR. Moreover, epitaxial engineering in core−shell systems has advanced remarkably over the past decade. This resulted in photochemically stable QDs with photoluminescence (PL) quantum yield close to unity.[3,4] Furthermore, the control over epitaxial core−shell synthesis enabled the community to explore new degrees of freedom brought by engineering of the exciton wave functions,[5] resulting in reduced Auger recombination,[6−8] brighter multiexciton emission, and lower lasing thresholds.[9−11] There is no doubt that following these recent advances, colloidal QDs will be used in a wide variety of applications, ranging from biological research[12−14] to luminescent light concentrators[15−17] and displays.[18]

Nowadays, two of the most important applications of colloidal QDs are their use as spectral conversion phosphors in light-emitting diodes (LEDs) and in (the backlight of) liquid crystal (LC) displays. In LEDs aimed at general lighting applications, the main role of QDs is to partially convert the primary blue light from the LEDs into multicolored light, with a spectrum matching human needs. In LED technology, where a high power efficiency is paramount, QDs have shown to be valuable for two different reasons: (i) they have a high quantum yield, and (ii) they are narrow band emitters. When QDs are used as a red phosphor instead of traditional wide-band red emitters, the red emission of an LED lamp is possible without losing photons in the near-IR, thereby significantly boosting the power efficacy (lumen/watt) of the lamp. Additionally, by using mixtures of differently colored QDs, it is relatively easy to achieve a high color rendering index lamp (CRI > 90), compared to traditional phosphors. Regarding display technology, QDs have shown to be valuable for their size-dependent tunable, narrow-band emission, which enables a strong matching of the backlight emission with the color filters of the display, thereby enhancing brightness and color saturation. In displays, QDs are already applied commercially. In order to strengthen these properties and enhance the suitability of QDs for industrial applications, especially for white light emission, several approaches have been proposed: QDs doped with metal ions,[19,20] ultrasmall CdSe QDs,[21,22] or QDs that show a

Received: June 7, 2017
Accepted: August 8, 2017
Published: August 8, 2017

DOI: 10.1021/acsnano.7b03975
ACS Nano 2017, 11, 9136−9142

relatively broad spectrum due to multiexciton emission[23] or shell emission.[24] All of these materials show only partially tunable emission spectra. Moreover, the spectra change with the intensity of the excitation, thus hampering several applications. A simple approach would be to mix three types of colloidal semiconductor QDs with emission in the red, green, and blue, respectively. In this respect, attempts based on mixed thin films of QDs have been reported.[25]

Here, we report an approach that results in spherical supraparticles (SPs) that are composed of QDs emitting in the red, green, and blue. By controlling the ratios of QDs per SP, we can easily and rationally tune the spectrum of the SPs, and the emission spectrum is independent of the excitation intensity in a wide range. The SPs are charge- and sterically stabilized colloids themselves and can be dispersed in many industrially relevant polar solvents, including water. In addition, their much larger size as compared to individual QDs also makes them easier to process in an industrial setting. Our work presents a platform for easily processable colloidal particles with a bright and stable (non-blinking) emission of pure or composite color, tunable in the entire visible range. Such a platform holds promise for displays as well as optoelectronical and biological applications.

RESULTS/DISCUSSION

Synthesis and Composition of the Tunable Emitting SPs. The first step in the realization of SPs is to synthesize the constituent QDs. For this, we adapted existing protocols for stable red, green, and blue emitting Cd(Se,ZnS) core/(Cd,Zn)S shell QDs (Figure 1) (see SI for further information).

Our general approach for the self-assembly of the SPs is based on the drying of an oil-in-water emulsion at elevated temperatures (68 °C) as described previously[26,27] (details given in the SI). In Figure S1 the synthesis procedure is schematically presented. The emulsification is performed through a methodology developed by the Bibette group that uses high shear rates generated in a Couette shear cell[28] combined with the viscoelasticity of a concentrated emulsion; this leads to fairly monodisperse breakup of the droplets. In this manner, SPs with a precise size can be produced in a size range between 100 nm and several micrometers (Figure.S2).

The three types of QDs that are incorporated in the SP are of similar size, and they have the same inorganic outer shell (ZnS) and organic ligands (oleic acid). However, the sizes are different enough that the effective polydispersity of the mixture is above 10%, which should prevent crystallization of the QDs into a long-range ordered superstructure. We therefore expect that the three types of QDs will be randomly packed and homogeneously distributed in the SPs in proportion to their concentration in the precursor suspension of mixed QDs.

Structural Characterization of the SPs. The surface structure of the as-prepared SPs can be studied by detection of secondary electrons (SE) in a scanning transmission electron microscope (STEM) (Figures 2a and S3). To investigate the inner structure of the SPs, high-angle annular dark-field scanning transmission electron microscopy (HAADF-STEM) is combined with electron tomography[29,30] (Figure 2b–e). Hereby, a tilt series of HAADF-STEM images (Figure 2b) is acquired along different viewing directions and is combined into a three-dimensional (3D) reconstruction (Figure 2c) using a mathematical algorithm (see SI). In Figure 2d we present a slice through the 3D reconstruction yielding the internal structure. This image as well as the fast Fourier transform in Figure 2e clearly show that the QDs are not ordered in the SPs, thus forming an amorphous glassy structure, as expected. In order to investigate the type of packing in the assemblies in more detail, the coordinates extracted from the tomography reconstruction were used to calculate bond order parameters.[31,32] The analysis excluded the presence of periodic arrangements of particles. It was shown previously[26] that if the composing QDs have the same size and a regular spherical shape and their interactions can be approximated well with that of a hard-sphere potential, then the SPs form crystalline structures with an icosahedral or face-centered cubic structure. In our case, the composing QDs mixtures are characterized by a relatively high polydispersity and an irregular shape; this leads to a random arrangement of the QDs inside the SPs with a high packing fraction. This is confirmed by the radial distribution function (RDF) (Figure S4), which is calculated through the identification of the single QDs inside a SP (Figure S5). The RDF shows an average distance between nearest neighbors of 10.9 nm, which is in agreement with the particle size derived from TEM images.

The 3D analysis of the SPs by electron tomography also enables us to verify whether the QDs are homogeneously mixed in each of the SPs. In Figure S6a–c, HAADF-STEM images acquired from the individual red, green, and blue population are presented. The shape of the red emitting QDs is more spherical in comparison to the other types. The intensity in HAADF-STEM images depends on the atomic number Z. Energy dispersive X-ray spectroscopy (EDS) measurements on the individual QDs (Figures S7–S10) show that the red emitting particles contain a higher amount of Cd in their structure compared to the green and blue ones (Table S1). In this manner, we conclude that the high intensity particles in the orthoslices correspond to red emitting particles. Visual inspection of the QDs in the orthoslices in Figure 2d shows that the different QDs are homogeneously mixed in each SP. The homogeneous distribution of the QDs in the SPs was further confirmed by EDS measurements (Figure S11). From Figure S11 it is clear that all the elements, and in particular Se (which is not present in the blue emitting QDs), were found to be homogeneously distributed inside the SP, thus supporting our statements about the homogeneous distribution of the QDs inside the SPs.

Optical Characterization of Individual SPs and Ensembles. We use confocal microspectroscopy to study the optical properties of our SPs (Figure 3). Microscopy of individual micron-sized SPs, larger than the diffraction limit, demonstrates that the emission of the red, blue, and green light does not vary spatially within a SP (Figures 3a,b and S12). This agrees with the homogeneous mixing of the QDs in each SP as derived from electron tomography measurements (see above). Confocal microscopy also confirms uniform emission spectra among all SPs in one batch. Even SPs from one synthesis batch but with different sizes show similar PL emission spectra (Figures 3c–e and S13).

Using (time-resolved) PL spectroscopy, we study in more detail how the ensemble-averaged optical properties of the SPs relate to those of the separate constituent QDs (Figure 4). In Figure 4a the emission spectra are compared. The contributions from the separate NC populations (colored lines) are clearly distinguished in the composite emission spectrum of the SP (black). This is to be expected because (i) the constituent QDs are too far apart to exhibit quantum mechanical coupling that could otherwise change the energy levels and (ii) the SPs are

DOI: 10.1021/acsnano.7b03975
ACS Nano 2017, 11, 9136–9142

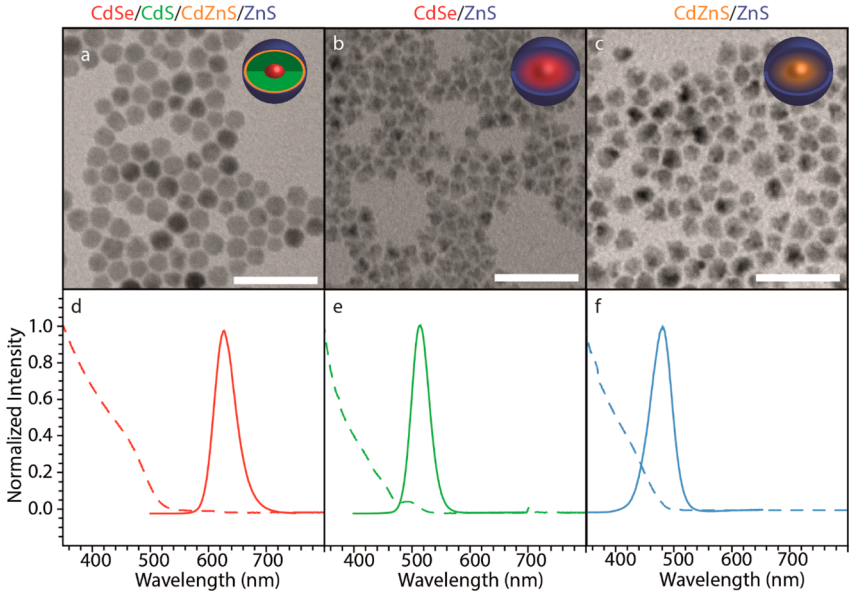

Figure 1. TEM images and optical properties of the original QDs. (a–c) Representative transmission electron micrographs (scale bar 50 nm) of (a) the red emitting QDs (diameter: 10.3 ± 1.0 nm), (b) the green emitting QDs (diameter: 11.0 ± 1.1 nm), and (c) the blue emitting QDs (diameter: 10.5 ± 1.3 nm). Insets are models of the QDs. (d–f) Absorption (dashed lines) and emission (solid lines) spectra of three different populations of QDs used for the self-assembly.

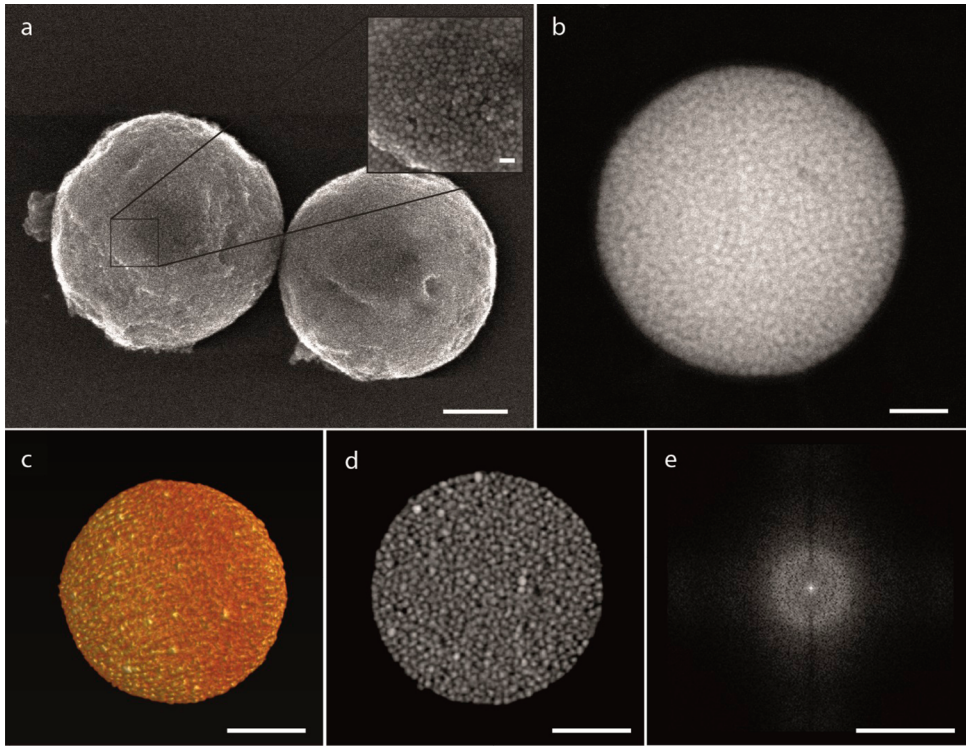

Figure 2. Structural characterization of the SPs. (a) SE-STEM image of two SPs (scale bar 200 nm). The inset shows a magnification of one of the particles (scale bar 20 nm). Individual QDs can be clearly distinguished. (b, c) 2D HAADF-STEM images (scale bars 50 nm) of a small SP for which electron tomography has been performed (b), and a 3D visualization of the 3D tomographic reconstruction of the same SP (c). (d) Slice through the center of the 3D reconstruction of the SP (scale bar 50 nm). Individual QDs can be clearly recognized as well as their relative position, showing the irregular inner structure. (e) Fast Fourier transform of the slice of panel d (scale bar 0.1 nm^{-1}).

too polydisperse for whispering gallery modes[27] to appear in the ensemble emission spectrum. Nevertheless, the peak position of the blue contribution to the SP emission (black line) is slightly red-shifted from the peak position of the dispersion of blue QDs (blue). This indicates energy transfer among blue QDs in the SP and/or from blue QDs to the green and red QDs. Most likely, both Förster-type energy transfer (*i.e.*, by dipole–dipole coupling) and photon reabsorption contribute to this. We wish to remark that the emission spectrum of the composed SPs is independent of the excitation intensity in the broad range of single exciton excitation (up to 14 mW) (Figure S14). This is an important asset compared to

DOI: 10.1021/acsnano.7b03975
ACS Nano 2017, 11, 9136–9142

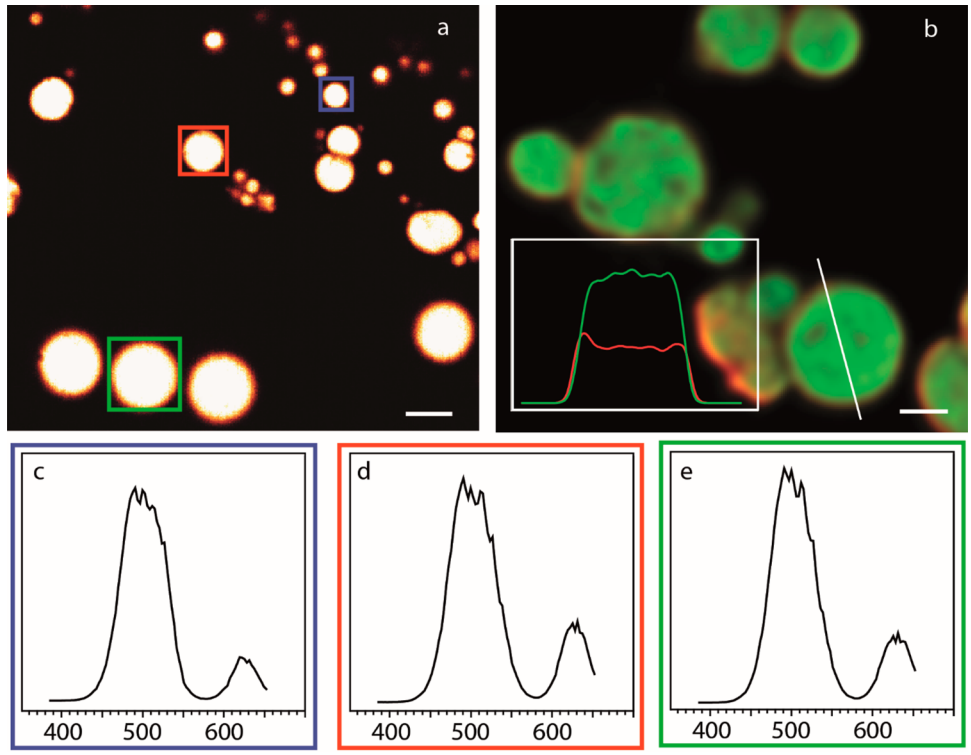

Figure 3. Optical characterization of the SPs. (a) Confocal microscopy image of a set of SPs drop-casted and dried on a glass slide and excited with UV excitation (scale bar 3 μm). (b) Confocal fluorescence image of different SPs (scale bar 1 μm). The blue-green emission (450−550 nm) is shown in green, while the red emission (600−700 nm) is shown in red; the image is deconvolved through the modeling of the point spread function of the microscope. The inset shows the signal collected along the white line drawn in the figure coming from the two detectors. (c−e) Emission spectra of some of the SPs presented in panel a, indicated with the green, red, or blue frame.

previous proposals in which a broad emission was reached by simultaneous exciton and biexciton emission[23] or shell emission.[24]

In Figure 4b−d we show the PL decay dynamics of the three batches of QDs freely dispersed in toluene (closed circles) compared to QDs assembled into a SP (open circles). The suspension of the red emitting QDs shows the slowest PL decay, followed by the green and the blue emitting QDs, qualitatively in agreement with the frequency dependence of the optical transition strengths.[33] The decay dynamics of the same batches of QDs assembled in water-dispersed SPs are consistently faster. More precisely, the PL of SPs consisting purely of red QDs (red open circles) decays 66% faster than that of freely dispersed QDs in toluene (see Supporting Information for a description of our analysis procedure). The decay of the red component in mixed white light-emitting SPs (black open circles) is 33% faster than the red NC dispersion. For the green emission, these acceleration factors are 41% for the purely green SPs and 32% for the mixed SPs; for the blue emission 29% and 211%.

Multiple collective effects simultaneously affect the decay dynamics in the SPs. For example, the local density of optical states (LDOS), which determines the rate of radiative decay, is higher for QDs in a SP than for those freely dispersed in toluene. We estimate the LDOS in a SP using a simplified model, where the SP is assumed to be a perfect sphere with a homogeneous refractive index, which can support Mie resonances (Figure S15). This model predicts that the LDOS, averaged over the volume of the SP and orientation of the transition dipole moments, is approximately two times larger in a SP than for free QDs (Figure S15). Indeed, the PL decay in SPs is always faster than for dispersed QDs (Figure 4b−d). However, the acceleration is less pronounced than the simplified Mie model predicts, which can in part be due to damping of the Mie resonances by refractive index inhomogeneities and absorption in the SP. Moreover, the PL decay dynamics observed can be affected by Förster energy transfer among QDs and reabsorption of emitted light.

We can get some insight into the occurrence of Förster energy transfer in the SPs by comparing the PL decay dynamics in pure-color SPs (colored open circles in Figure 4b−d) and mixed white light SPs (gray open circles). In pure-color SPs energy transfer can occur only among QDs from the same (inhomogeneously broadened) color population. Mixed SPs enable additional transfer between populations from blue to green, blue to red, and green to red. Indeed, the blue PL decay (Figure 4d) is faster in mixed SPs than in pure SPs because of these additional decay channels. The red PL (Figure 4b) is slower in mixed SPs, because the red QDs are fed through energy transfer from the blue and green populations. The green PL decay is approximately equally fast in pure and mixed SPs, which indicates that the effects of feeding from the blue population and transfer to the red compensate each other. Detailed modeling of these energy-transfer processes and their effect on the color output depends on many factors (*e.g.*, the degree of inhomogeneous broadening and the separations and relative orientations of the QDs in the SP). This is beyond the scope of the current work. Nevertheless, these effects must be taken into account in the composition of the SPs if a certain desired shade of white light is targeted (see below), and in our case this was done empirically.

DOI: 10.1021/acsnano.7b03975
ACS Nano 2017, 11, 9136−9142

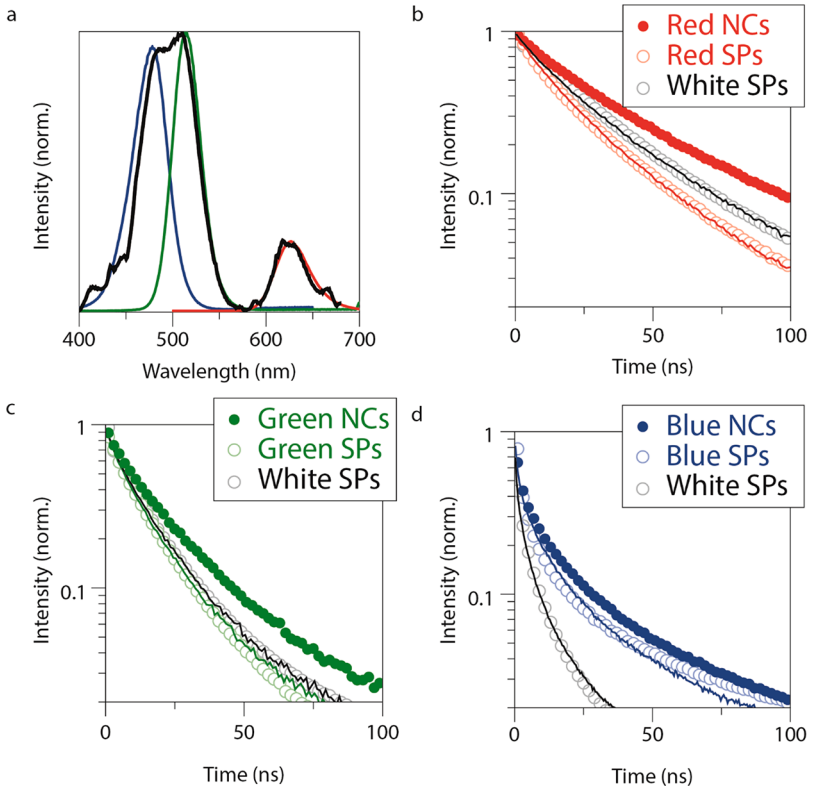

Figure 4. Optical properties of SPs compared to suspensions of the constituent QDs. (a) Emission spectrum of an ensemble of white light-emitting SPs (black) and of the three separate dispersions of the constituent QDs (colored; each scaled to match the maximum intensity of the corresponding peak in the composite spectrum). (b) PL decay traces of red QDs freely dispersed in toluene (red closed circles), assembled in water-dispersed SPs of red QDs (red open circles), and assembled in a white light-emitting SPs (gray open circles). The red line is a fit to the PL decay of red SPs, and the black line to the decay of white-light emitting SPs (see Supporting Information for an explanation of the fitting procedure). Same for (c) green QDs and (d) blue QDs.

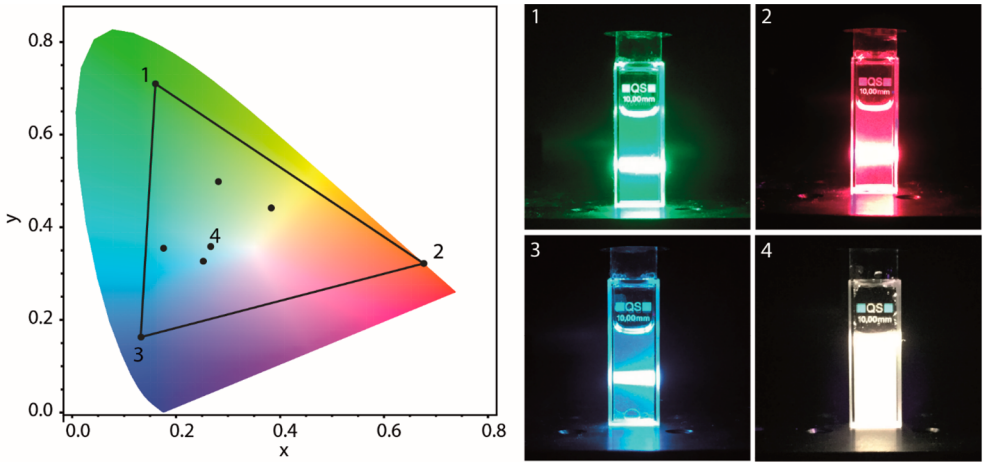

Figure 5. CIE chromaticity diagram of the QDs and the SPs. Left: CIE diagram representing different SP batches as obtained by changing the ratio between the three QDs populations. The vertices of the triangle represent the coordinates of the three types of QDs. Therefore, the area of the triangle represents all the possible colors SPs can have. Right (1−3): Digital true-color photographs of the QDs dispersed in solution when illuminated with a UV laser. (4) Digital photograph of a dispersion of the SPs, composed of the three types of QDs, emitting white light.

Lighting applications require photochemically stable SPs, while many biolabeling applications require time-constant emission from individual SPs, without blinking or dark periods. Our SPs show bright, non-blinking, and non-bleaching emission on the single-SP level over a time period of at least 3000 s (Figure S16). This stability is an important asset compared to conventional optical labels, for example, silica particles filled with organic dyes such as rhodamine isothiocyanate (RITC).[34]

Concerning the non-blinking feature, we remark that this is due to the concomitant emission of many QDs in each SP. We also remark that the size of the SPs can be tuned up to 100 nm, that they can be dispersed in water, if needed, coated by a thin silica layer, and that the surface can be biofunctionalized at will. Thus, the NC SPs presented here, emitting one color or a combination of two or three fundamental colors, are suitable as biological labels.

DOI: 10.1021/acsnano.7b03975
ACS Nano 2017, 11, 9136−9142

For application of the SPs as spectral conversion phosphors in lighting, the precise tunability of the white light spectrum is of great importance. To study this, we convert the pure spectra of the constituent QDs and the composite spectra of the SPs to coordinates of the Commission Internationale de l'Éclairage (CIE) chromaticity space (Figure 5). The vertices of the triangle are the coordinates of the three QDs components. The better the color purity of the single NC components, the larger the area of the triangle in the CIE space. The area inside the triangle represents all the colors that can be achieved by composing SPs from the three different QDs used here. The color purity of the QDs, as used here, is another important advantage of NC SPs over regular phosphors that usually have a broad emission spectrum. The black dots within the triangle in Figure 5 represent color points that we obtained by assembling our QDs into SPs. A given broad SP emission spectrum can be achieved and fine-tuned if one knows the emissive strength of the red, green, and blue emitting QDs and takes the lower effective emission yield from the blue-emitting particles into account, in a few experimental iterations (see Figure S17). We remark that a targeted composite emission spectrum will remain independent of excitation intensity over a broad excitation regime as long as the steady-state exciton population remains below unity.

CONCLUSIONS

We have reported the synthesis and structural and optical characterization of colloidal water-soluble SPs composed of three types of QDs. The SPs can be fabricated to emit pure colors as well as a broad white light spectrum (or anything in between) that can be fine-tuned *via* the NC composition of the SPs. The bright emission from individual SPs is stable over time and does not blink. Such SPs hold promise as phosphors in LEDs for lighting, opto-electrical integration in semiconductor chips and as biological labels.

METHODS

Synthesis of QDs. Three different populations of Cd(Se,ZnS) core/(Cd,Zn,S) shell QDs emitting in different regions of the visible spectrum were synthesized according to a modified literature procedure.[35−37] For further details about the synthesis and characterization procedure see the Supporting Information. The QDs were precipitated by centrifugation with the addition of a MeOH:BuOH 3:1 v/v solution and redispersed in cyclohexane to form stock solutions with a concentration of 8−15 mg/mL.

Synthesis of SPs. For the SPs, the three different solutions of core/shell QDs were mixed in the desired ratio to a total volume of 1 mL and then mixed with 10 mL water containing sodium dodecyl sulfate and dextran. The mixture was sheared at a shear rate of 7×10^3 s^{-1} in a shear cell with a gap of 0.1 mm, and the resulting oil-in-water emulsion was heated at 68 °C for 4 h. The resulting SPs were precipitated by centrifugation, and the supernatant, containing surfactants and dextran in excess, was discarded. SPs were redispersed in deionized water. For a detailed description of the methods and equipment used, see the Supporting Information.

Electron Microscopy. HAADF-STEM images, SE-STEM images, EDS maps, and electron tomography series of the SPs were acquired using a FEI Osiris and a FEI Tecnai electron microscopes operated at 200 kV. Electron tomography series were acquired by using a Fischione model 2020 single tilt tomography holder. The series were acquired within the tilt ranges from −64° to +74° and from −76° to +64° and a tilt increment of 2°. For the reconstruction of the series, the simultaneous iterative reconstruction technique (SIRT) was used, implemented in the ASTRA toolbox.[38−40]

HAADF-STEM images and EDS maps of the QDs were acquired using an aberration-corrected "cubed" FEI Titan 60−300 electron microscope operated at 120 kV, equipped with a ChemiSTEM[41] system.

ASSOCIATED CONTENT

Supporting Information

The Supporting Information is available free of charge on the ACS Publications website at DOI: 10.1021/acsnano.7b03975.

Synthesis of core/multishell QDs, optical characterization of the QDs, synthesis of the SPs, determination of the quantum yield of QDs and SPs, determination of the RDF and CIE coordinates (PDF)

AUTHOR INFORMATION

Corresponding Author

*E-mail: d.vanmaekelbergh@uu.nl.

ORCID

Sara Bals: 0000-0002-4249-8017

Daniel Vanmaekelbergh: 0000-0002-3535-8366

Notes

The authors declare no competing financial interest.

ACKNOWLEDGMENTS

We thank J. J. Geuchies for help with the optical analysis, W. Vlug for providing silica particles filled with RITC, J. D. Meeldijk for his assistance with SE-STEM measurements, E. B. van der Wee for help with the calculation of the radial distribution functions, and M. van Huis and S. Dussi for very fruitful discussions. This work was supported by the European Comission *via* the Marie-Sklodowska Curie action Phonsi (H2020-MSCA-ITN-642656). D.V. wishes to thank the Dutch FOM (program DDC13), NWO−CW (Toppunt 718.015.002), and the European Research Council under HORIZON 2020 (grant 692691 FIRSTSTEP) for financial support. A.v.B. and F.M. acknowledge partial funding from the European Research Council under the European Union's Seventh Framework Programme (FP-2007-2013)/ERC advanced grant agreement 291667: HierarSACol. S.B. and D.Z. acknowledge financial support from the European Research Council (starting grant no. COLOURATOM 335078), and T.A. acknowledges funding from the Research Foundation Flanders (FWO, Belgium) through a postdoctoral grant.

REFERENCES

(1) Murray, C. B.; Norris, D.; Bawendi, M. G. Synthesis and Characterization of Nearly Monodisperse CdE (E S, Se, Te) Semiconductor Nanocrystallites. *J. Am. Chem. Soc.* **1993**, *115*, 8706−8715.

(2) Talapin, D. V.; Lee, J. S.; Kovalenko, M. V.; Shevchenko, E. V. Prospects of Colloidal Nanocrystals for Electronic and Optoelectronic Applications. *Chem. Rev.* **2010**, *110*, 389−458.

(3) Chen, O.; Zhao, J.; Chauhan, V. P.; Cui, J.; Wong, C.; Harris, D. K.; Wei, H.; Han, H.-S.; Fukumura, D.; Jain, R. K.; Bawendi, M. G. Compact High-Quality CdSe-CdS Core-Shell Nanocrystals with Narrow Emission Linewidths and Suppressed Blinking. *Nat. Mater.* **2013**, *12*, 445−451.

(4) Christodoulou, S.; Vaccaro, G.; Pinchetti, V.; De Donato, F.; Grim, J. Q.; Casu, a.; Genovese, a.; Vicidomini, G.; Diaspro, a.; Brovelli, S.; Manna, L.; Moreels, I. Synthesis of Highly Luminescent Wurtzite CdSe/CdS Giant-Shell Nanocrystals Using a Fast Continuous Injection Route. *J. Mater. Chem. C* **2014**, *2*, 3439.

DOI: 10.1021/acsnano.7b03975
ACS Nano 2017, 11, 9136−9142

(5) de Mello Donegá, C. Synthesis and Properties of Colloidal Heteronanocrystals. *Chem. Soc. Rev.* **2011**, *40*, 1512−1546.
(6) García-Santamaría, F.; Chen, Y.; Vela, J.; Schaller, R. D.; Hollingsworth, J. a; Klimov, V. Suppressed Auger Recombination in "Giant" Nanocrystals Boosts Optical Gain Performance. *Nano Lett.* **2009**, *9*, 3482−3488.
(7) Mahler, B.; Spinicelli, P.; Buil, S.; Quelin, X.; Hermier, J.-P.; Dubertret, B. Towards Non-Blinking Colloidal Quantum Dots. *Nat. Mater.* **2008**, *7*, 659−664.
(8) Hollingsworth, J. A. Heterostructuring Nanocrystal Quantum Dots toward Intentional Suppression of Blinking and Auger Recombination. *Chem. Mater.* **2013**, *25*, 1318−1331.
(9) Park, Y.-S.; Bae, W. K.; Baker, T.; Lim, J.; Klimov, V. I. Effect of Auger Recombination on Lasing in Heterostructured Quantum Dots with Engineered Core/Shell Interfaces. *Nano Lett.* **2015**, *15*, 7319−7328.
(10) Klimov, V. I.; Mikhailovsky, a. a.; Xu, S.; Malko, a; Hollingsworth, J. a.; Leatherdale, C. a; Eisler, H.-J.; Bawendi, M. G. Optical Gain and Stimulated Emission in Nanocrystal Quantum Dots. *Science (Washington, DC, U. S.)* **2000**, *290*, 314−317.
(11) Klimov, V. Spectral and Dynamical Properties of Multiexcitons in Semiconductor Nanocrystals. *Annu. Rev. Phys. Chem.* **2007**, *58*, 635−673.
(12) Alivisatos, P. The Use of Nanocrystals in Biological Detection. *Nat. Biotechnol.* **2004**, *22*, 47−52.
(13) Bruchez, M., Jr.; Moronne, M.; Gin, P.; Weiss, S.; Alivisatos, A. P. Semiconductor Nanocrystals as Fluorescent Biological Labels. *Science* **1998**, *281*, 2013−2016.
(14) Michalet, X.; Pinaud, F.; Bentolila, L.; Tsay, J.; Doose, S.; Li, J.; Sundaresan, G.; Wu, A.; Gambhir, S.; Weiss, S. Quantum Dots for Live Cells, *in Vivo* Imaging, and Diagnostics. *Science (Washington, DC, U. S.)* **2005**, *307*, 538−544.
(15) Meinardi, F.; McDaniel, H.; Carulli, F.; Colombo, A.; Velizhanin, K. a.; Makarov, N. S.; Simonutti, R.; Klimov, V. I.; Brovelli, S. Highly Efficient Large-Area Colourless Luminescent Solar Concentrators Using Heavy-Metal-Free Colloidal Quantum Dots. *Nat. Nanotechnol.* **2015**, *10*, 878−885.
(16) Meinardi, F.; Colombo, A.; Velizhanin, K. a.; Simonutti, R.; Lorenzon, M.; Beverina, L.; Viswanatha, R.; Klimov, V.; Brovelli, S. Large-Area Luminescent Solar Concentrators Based on "Stokes-Shift-Engineered" Nanocrystals in a Mass-Polymerized PMMA Matrix. *Nat. Photonics* **2014**, *8*, 392−399.
(17) Bradshaw, L. R.; Knowles, K. E.; McDowall, S.; Gamelin, D. R. Nanocrystals for Luminescent Solar Concentrators. *Nano Lett.* **2015**, *15*, 1315−1323.
(18) Shirasaki, Y.; Supran, G. J.; Bawendi, M. G.; Bulović, V. Emergence of Colloidal Quantum-Dot Light-Emitting Technologies. *Nat. Photonics* **2013**, *7*, 13−23.
(19) Kim, J.-H.; Jo, D.-Y.; Lee, K.-H.; Jang, E.-P.; Han, C.-Y.; Jo, J.-H.; Yang, H. White Electroluminescent Lighting Device Based on a Single Quantum Dot Emitter. *Adv. Mater.* **2016**, *28*, 5093−5098.
(20) Panda, S. K.; Hickey, S. G.; Demir, H. V.; Eychmüller, A. Bright White-Light Emitting Manganese and Copper Co-Doped ZnSe Quantum Dots. *Angew. Chem.* **2011**, *123*, 4524−4528.
(21) Schreuder, M. A.; Xiao, K.; Ivanov, I. N.; Weiss, S. M.; Rosenthal, S. J. White Light-Emitting Diodes Based on Ultrasmall CdSe Nanocrystal Electroluminescence. *Nano Lett.* **2010**, *10*, 573−576.
(22) Bowers, M. M. J.; Ii, M. J. B.; McBride, J. R.; Rosenthal, S. J. White-Light Emission from Magic-Sized Cadmium Selenide Nanocrystals. *J. Am. Chem. Soc.* **2005**, *127*, 15378−15379.
(23) Nasilowski, M.; Spinicelli, P.; Patriarche, G.; Dubertret, B. Gradient CdSe/CdS Quantum Dots with Room Temperature Biexciton Unity Quantum Yield. *Nano Lett.* **2015**, *15*, 3953−3958.
(24) Brovelli, S.; Bae, W. K.; Galland, C.; Giovanella, U.; Meinardi, F.; Klimov, V. I. Dual-Color Electroluminescence from Dot-in-Bulk Nanocrystals. *Nano Lett.* **2014**, *14*, 486−494.
(25) Lee, K.; Han, C.; Kang, H.; Ko, H.; Lee, C.; Lee, J.; Myoung, N.; Yim, S.-Y.; Yang, H. Highly Efficient, Color-Reproducible Full-Color Electroluminescent Devices Based on Red/Green/Blue Quantum Dot-Mixed Multilayer. *ACS Nano* **2015**, *9*, 10941−10949.
(26) de Nijs, B.; Dussi, S.; Smallenburg, F.; Meeldijk, J. D.; Groenendijk, D. J.; Filion, L.; Imhof, A.; Dijkstra, M.; Van Blaaderen, A. Entropy-Driven Formation of Large Icosahedral Colloidal Clusters by Spherical Confinement. *Nat. Mater.* **2015**, *14*, 56−60.
(27) Vanmaekelbergh, D.; van Vugt, L. K.; Bakker, H.; Rabouw, F. T.; de Nijs, B.; van Dijk-Moes, R.; Beasjou, P.; Van Blaaderen, A. Shape-Dependent Multiexciton Emission and Whispering Gallery Modes in Supraparticles of CdSe/Multishell Quantum Dots. *ACS Nano* **2015**, *9*, 3942−3950.
(28) Mabille, C.; Schmitt, V.; Gorria, P.; Leal Calderon, F.; Faye, V.; Deminière, B.; Bibette, J. Rheological and Shearing Conditions for the Preparation of Monodisperse Emulsions. *Langmuir* **2000**, *16*, 422−429.
(29) Midgley, P. a.; Weyland, M. 3D Electron Microscopy in the Physical Sciences: The Development of Z-Contrast and EFTEM Tomography. *Ultramicroscopy* **2003**, *96*, 413−431.
(30) Altantzis, T.; Goris, B.; Sánchez-Iglesias, A.; Grzelczak, M.; Liz-Marzán, L. M.; Bals, S. Quantitative Structure Determination of Large Three-Dimensional Nanoparticle Assemblies. *Part. Part. Syst. Charact.* **2013**, *30*, 84−88.
(31) Steinhardt, P. J.; Nelson, D. R.; Ronchetti, M. Bond-Orientational Order in Liquids and Glasses. *Phys. Rev. B: Condens. Matter Mater. Phys.* **1983**, *28*, 784−805.
(32) Wang, Y.; Teitel, S.; Dellago, C. Melting of Icosahedral Gold Nanoclusters from Molecular Dynamics Simulations. *J. Chem. Phys.* **2005**, *122*, 214722.
(33) van Driel, A. F.; Allan, G.; Delerue, C.; Lodahl, P.; Vos, W. L.; Vanmaekelbergh, D. Frequency-Dependent Spontaneous Emission Rate from CdSe and CdTe Nanocrystals: Influence of Dark States. *Phys. Rev. Lett.* **2005**, *95*, 236804.
(34) Verhaegh, N. A. M.; van Blaaderen, A. Dispersions of Rhodamine-Labeled Silica Spheres: Synthesis, Characterization, and Fluorescence Confocal Scanning Laser Microscopy. *Langmuir* **1994**, *10*, 1427−1438.
(35) Li, J. J.; Wang, Y. A.; Guo, W.; Keay, J. C.; Mishima, T. D.; Johnson, M. B.; Peng, X. Large-Scale Synthesis of Nearly Monodisperse CdSe/CdS Core/Shell Nanocrystals Using Air-Stable Reagents *via* Successive Ion Layer Adsorption and Reaction. *J. Am. Chem. Soc.* **2003**, *125*, 12567−12575.
(36) Bae, W. K.; Kwak, J.; Park, J. W.; Char, K.; Lee, C.; Lee, S. Highly Efficient Green-Light-Emitting Diodes Based on CdSe@ZnS Quantum Dots with a Chemical-Composition Gradient. *Adv. Mater.* **2009**, *21*, 1690−1694.
(37) Lee, K.; Lee, J.; Song, W.; Ko, H.; Lee, C.; Lee, J.; Yang, H. Higly Efficient, Color-Pure, Color-Stable Blue Quantum Dot Light-Emitting Devices. *ACS Nano* **2013**, *7*, 7295−7302.
(38) van Aarle, W.; Palenstijn, W. J.; De Beenhouwer, J.; Altantzis, T.; Bals, S.; Batenburg, K. J.; Sijbers, J. The ASTRA Toolbox: A Platform for Advanced Algorithm Development in Electron Tomography. *Ultramicroscopy* **2015**, *157*, 35−47.
(39) van Aarle, W.; Palenstijn, W. J.; Cant, J.; Janssens, E.; Bleichrodt, F.; Dabravolski, A.; Beenhouwer, J. De; Batenburg, K. J.; Sijbers, J. Fast and Flexible X-Ray Tomography Using the ASTRA Toolbox. *Opt. Express* **2016**, *24*, 25129−25147.
(40) Palenstijn, W. J.; Batenburg, K. J.; Sijbers, J. Performance Improvements for Iterative Electron Tomography Reconstruction Using Graphics Processing Units (GPUs). *J. Struct. Biol.* **2011**, *176*, 250−253.
(41) Schlossmacher, P.; Klenov, D. O.; Freitag, B.; von Harrach, H. S. Enhanced Detection Sensitivity with a New Windowless XEDS System for AEM Based on Silicon Drift Detector Technology. *Microsc. Today* **2010**, *18*, 14−20.

DOI: 10.1021/acsnano.7b03975
ACS Nano 2017, 11, 9136−9142